A Fast in Silico Simulation of Ion Flux through the Large-Pore Channel Proteins

Sharron Bransburg-Zabary, Esther Nachliel, and Menachem Gutman
Laser Laboratory for Fast Reactions in Biology, Department of Biochemistry, The George S. Wise Faculty of Life Sciences, Tel Aviv University, Ramat Aviv 69978, Israel

ABSTRACT The PSST program (see accompanying article) utilizes the detailed structure of a large-pore channel protein as the sole input for selection of trajectories along which negative and positive ions propagate. In the present study we applied this program to reconstruct the ion flux through five large-pore channel proteins (PhoE, OmpF, the WT *R. blastica* general diffusion porin and two of its mutants). The conducting trajectories, one for positive and one for negative particles, are contorted pathways that run close to arrays of charged residues on the inner surface of the channel. In silico propagation of the charged particles yielded passage time values that are compatible with the measured average passage time of ions. The calculated ionic mobilities are close to those of the electrolyte solution of comparable concentrations. Inspection of the transition probabilities along the channel revealed no region that could impose a rate-limiting step. It is concluded that the ion flux is a function of the whole array of local barriers. Thus, the conductance of the large-pore channel protein is determined by the channel's shape and charge distribution, while the selectivity also reflects the features of the channel's vestibule.

INTRODUCTION

In the accompanying article we probed the intra-cavity aqueous phase of the PhoE channel by a single, free diffusing proton. The observed signal was analyzed by the geminate recombination formalism (Agmon, 1988; Agmon et al., 1988; Agmon and Szabo, 1990) using the structure of the protein as input for calculating the electrostatic potentials inside the channel. The potential maps were then evaluated by the PSST algorithm, looking for the most probable trajectory to be taken by the released proton. Finally, in silico calculations were used to propagate the proton along the trajectory, a procedure that reconstructs the observed experimental signal. An extensive search in the parameter space revealed that the accurate reconstruction was attained with $\epsilon_{\text{int-cav}} = 50 \pm 5$, very close to the value predicted by Sansom (Breed et al., 1996), that is significantly smaller than the dielectric constant of bulk water $\epsilon = 80$.

The precise reconstruction of the fluorescence decay dynamics of a pyranine molecule, located at a defined domain inside the PhoE channel, might be criticized as a refinement of parameters to fit a special case rather than a solution of a general problem. To test whether the PSST program is applicable for reconstruction of the ion flux in large-pore channels, in the present work we studied whether the same procedure can reconstruct the passage of either negative or positive ions through five ionic channels (PhoE, OmpF, and the WT plus two mutated general diffusion porins of *R. blastica*), whose structure and single-channel conductance had been published. For each of the channel proteins we calculated the electrostatic potential maps, selected the trajectories, and propagated positive and negative charges through them (in silico). The accuracy of the calculations was estimated by comparison between the measured single-channel conductance and the computed average passage times.

The propagation of ions through the large-pore channel protein had been investigated by detailed Brownian motion calculations (Phale et al., 2001; Schirmer and Phale, 1999) or, in the case of the narrow gauge gramicidin channel, through the Nernst-Plank procedure (Kurnikova et al., 1999). Both procedures were based on detailed reconstruction of the intra-cavity electrostatic potential and necessitated heavy computations, when most of the time (Jakobsson, 1998) is wasted on propagation of particles that were stuck in a potential well or those that refused to enter the channel pore. The present study avoids these limitations by focusing on particles that are already in the channel space, and follow a trajectory selected to avoid futile directions. Another simplification is attained by limiting the calculation to a single particle present in the channel. As will be shown below, a good fit (less than a factor of 2) was obtained for all cases without any need for adjustable parameters.

The selectivity and conductance of channels is traditionally attributed to two domains. The first one is the vestibule of the channel (Jordan, 1984; Partenski, 1992; Chung et al., 1998; Hoyles et al., 1996; Kuyucak et al., 1998), where the curvature of the dielectric boundary generates intensive electrostatic forces. Indeed, the recent Brownian motion calculations of Schirmer and Phale (Schirmer and Phale, 1999; Phale et al., 2001) indicated that only a small fraction of the ions, released at the vestibule, actually enter the channel's space. The second regulatory site was attributed to the eyelet of the channel, where the passage is constricted

Submitted February 4, 2002, and accepted for publication July 10, 2002.

Address reprint requests to Menachem Gutman, The George S. Wise Faculty of Life Sciences, Tel Aviv University, Ramat Aviv 69978, Israel. Tel.: 972-3-640-9875; Fax: 972-3-640-6834; E-mail: me@hemi.tau.ac.il.

S. Bransburg-Zabary's present address is Bioinformatics Unit, The George S. Wise Faculty of Life Sciences, Tel Aviv University.

0006-3495/02/12/3001/11 $2.00

by the protrusion of the L3 loop into the channel's lumen (Benz et al., 1989; Eppens et al., 1997; Vangelder et al., 1996). In the present study we wished to focus only on the role of the internal space in regulating the ion flux. For this reason, we deliberately restricted the analysis to ions that have already entered the channel's space, thus avoiding screening at the vestibule. In practice, the charged particles were irreversibly injected into a local reservoir set at the entry port without allowing them to be dispersed to the bulk. From the time point of injection, the probability density of the particle was calculated as a function of time and place until their probability density, past the exit port of the channel, reached the value of one.

The ion flux at each step along the channel is a product of two terms: the transition probability between consecutive sites and the local probability density of the particles. The transition probability is a time-independent term and is affected by the gradients of both electrostatic potential and entropy. The probability density along the trajectory is a time-dependent function, reflecting the temporal incoming and outgoing fluxes. The summation of all events along the trajectory yields the overall flux, and is thus affected both by upstream and downstream events.

Past modeling of ion flux in a large-pore channel (Smart et al., 1997; Benz and Buer, 1988) assumed that the total space of the channel is equally conductive. These calculations, which were based on Ohmic conductance, indicated that the conductivity inside the channel is ~30% of the bulk conductance of the same electrolyte solution, which was attributed to limited mobility of the ion in the constriction zone. The introduction of the trajectory concept avoids the difficulty to explain the limited diffusivity, replacing it by electrostatic confinement of the trajectory into a narrow pathway that occupies only a small fraction of the intra-channel space. The comparison between the calculated passage times and the measured single-channel conductance indicates that the effective diffusion coefficient of the ions along their trajectories is comparable to their diffusion coefficient in water. The normal diffusivity of the ions is in accord with the high activity of water in the channel (see accompanying article).

The standard ionic mobility of ions in the channel implies that there is no specific rate-limiting step along the pathway that imposes a bottleneck on the passage. More likely, the propagation of ions in the large-pore channels is regulated along the whole length of the conducting pathway, and is not limited to the eyelet region.

METHODS

Calculation of the intra-channel electrostatic potential

The calculation was based on the PDB files of the large-pore channel proteins 1PHO, 1OPF, 1PRN, 2PRN, and 6PRN for the PhoE, OmpF, and the WT *R. blastica* general diffusion porin and two of its mutants of the E99W/A116W (2PRN) and K50A/R52A (6PRN) (Schmid et al., 1998). All calculations were carried out on a single monomer rather than on trimers.

The electrostatic potential inside the channel was calculated by the DelPhi program with a spatial resolution of 0.33 Å, as described in the accompanying article. The protein was assigned with a dielectric constant of $\epsilon = 2$, the aqueous phase in the channel was characterized by $\epsilon_{\text{intra-cavity}} = 50$, and the water in the bulk by $\epsilon = 80$. The potentials were calculated for the ionic strength of the solutions used in the single-channel conductance measurements (generally 1 M), and the external field was superpositioned over the internal one (Pomes and Roux, 1996) as specified for each case.

The protein-ion interface was defined as the surface of closest approach of a sphere having a radius of $r = 2$ Å. The electrostatic potential maps were searched for local ion traps, sites from which the probability of propagation to the adjacent one was <5% (potential that is 3 k_BT below the adjacent sites). When a trap was identified, it was filled by an explicit ion and the whole procedure of mapping the electrostatic potential was repeated. This procedure was used mainly for precaution because, of the five channel proteins, only the PhoE was noticed to have an anion trap, very close to the site favored by the pyranine (see accompanying article).

Defining the trajectory

The trajectories were calculated separately, either for negative or positive charge, by the propagation along a structure supported trajectory (PSST) algorithm, as detailed in the accompanying article. The transition probabilities between the sites were calculated according to the electrostatic potential and entropic terms of each pair of consecutive sites.

Defining the boundary conditions

The calculations were carried out for a single charged particle that was irreversibly injected into a virtual reservoir (port of entry) located either at the extracellular or the periplasmic side of the channel. This virtual reservoir can be equated with a postvestibular locus, as the particle could not escape from the reservoir into the adjacent bulk phase. Thus, the present calculations are free of the selectivity pressure at the bulk-vestibule junction. The rate constant for the particle's transfer into the channel space was $k_{\text{in}} = 10^{10}\ \text{s}^{-1}$, set to be fast enough not to be a rate-limiting step. To account for the electrostatic potential at the port of entry, the particle could re-enter the reservoir at a rate constant (k_{res}) that is proportional to the potential difference (ΔE_1) between the channel's port and the reservoir ($k_{\text{res}} = k_{\text{in}} \exp(-\Delta E_1/k_BT)$. As both rate constants are very fast, a quasi-equilibrium between the reservoir and the channel is established within a fraction of a nanosecond.

A particle that propagated all the way to the exit port, on the other side of the channel, was accumulated in an acceptor reservoir, and considered to be irreversibly lost in the bulk. The dynamics of the accumulation of the particle's probability density at the bulk was recorded as a function of the number of random steps executed by the system.

The ionic selectivity of large-pore channels is measured experimentally by imposing a salt gradient across the membrane (100 vs. 10 mM) and measuring the potential when the ion flux is reduced to zero (zero current potential). The ratio of the ion diffusivities is then calculated from the zero current potential by the Goldman-Hodgkin-Katz equation. The present equivalent of ionic selectivity was calculated under the following conditions: 1) the intra-channel electrostatic potential was calculated according to the highest salt concentration used in the measurements (100 mM); 2) the lower electrolyte concentration (10 mM) at the exit port was represented by a semi-absorbing boundary and reflected 10% of the particles back to the channel's space; 3) the ion entry was permitted only from the extracellular port and the ratio of the passage times (see below), calculated for positive and negative particles, was equated with the ionic selectivity of the channel.

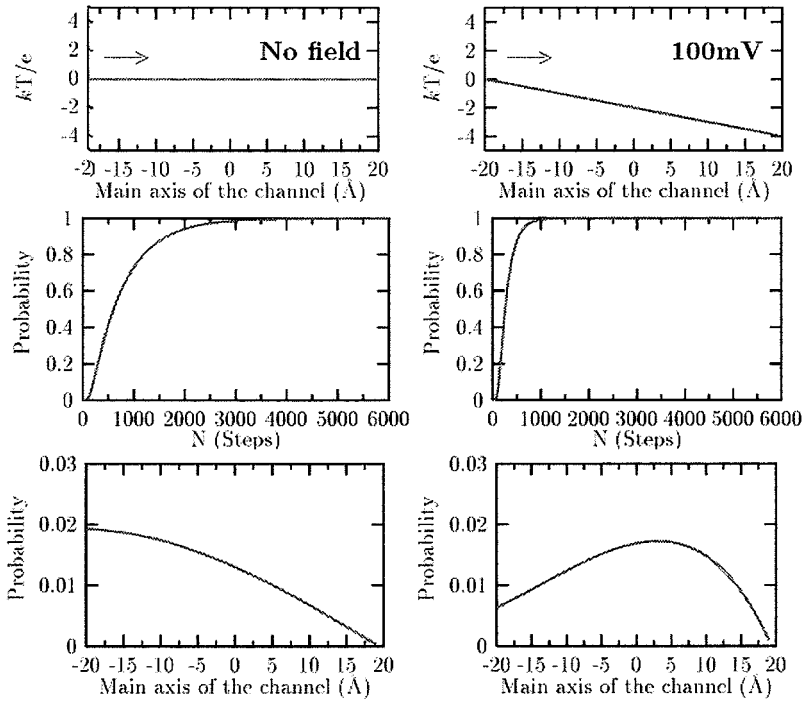

FIGURE 1 Propagation of a particle along a flat schematic trajectory in the absence and presence of an external electric field. The left panels were calculated for a 40-Å-long trajectory having no internal electric field and constant entropic terms (*top panel*). The mid-panel depicts the eviction dynamics of a single particle, irreversibly injected at the left side of the trajectory ($Z = -20$) and irreversibly absorbed on the right side ($Z = 20$). The accumulation of the particle's probability density past the exit port is presented as a function of the number of random steps taken by the system. The bottom panel depicts the probability density along the trajectory after $N_{1/2}$ random steps. The right panel depicts the same features under a driving potential of 100 mV (4 k_BT).

Propagation of the charged particles

The particles were propagated one at a time, as a single particle in the channel, using the transition probabilities calculated by the energy profile and the entropic terms of the particle's trajectory. We did not consider any ion-ion correlation or the effect of the particle charge on the intra-channel electrostatic potential.

The dynamics of the particle's escape out of the channel space was calculated as a function of the number of random steps. The rate of the process was calculated not in time units, but rather in a dimensionless parameter, the number of random steps ($N_{1/2}$) needed for the particle's probability density, which was accumulated past the exit port, reached the level of 50%. This mode of calculation circumvents the need for the precise value of the diffusion coefficient. A large value of $N_{1/2}$ corresponds with a slow passage, and the smaller it is, the faster the passage. In single-channel conductance measurements, carried out in black lipid membrane (Benz et al., 1985; Menzl et al., 1996), the protein is incorporated from both sides of the membrane, so we can assume unsiothropic orientation of the channels.

The measured current is the summation of the ionic mobilities of both anions and cations flowing in both directions. In accordance, the average passage time (τ) is correlated with the passage time of the positive and negative ions (τ^+ and τ^-, respectively) for each orientation of the protein in the membrane. (marked as $\tau^{-\,(\leftarrow)}$ and $\tau^{-\,(\rightarrow)}$) according to Eq. 1.

$$\tau^{-1} = \tfrac{1}{2}\{(\tau^{+(\rightarrow)})^{-1} + (\tau^{-(\leftarrow)})^{-1}\} + \tfrac{1}{2}\{(\tau^{+(\leftarrow)})^{-1} + (\tau^{-(\rightarrow)})^{-1}\} \quad (1)$$

The equivalent value of τ is the dimensionless parameter $\underline{N}_{1/2}$, which is related to $N_{1/2}$ (see above) as defined by the transformation of Eq 1 into

$$\underline{N}_{1/2}^{-1} = \tfrac{1}{2}\{(N_{1/2}^{+(\rightarrow)})^{-1} + (N_{1/2}^{-(\leftarrow)})^{-1}\} + \tfrac{1}{2}\{(N_{1/2}^{+(\leftarrow)})^{-1} + (N_{1/2}^{-(\rightarrow)})^{-1}\} \quad (2)$$

RESULTS

Propagation of particle in model trajectory

To evaluate how the profile of the electrostatic potential and the entropic terms affect the propagation of a particle, we modeled the simple trajectories presented in Figs. 1–3 and investigated how they modulate the passage of the charged particles. The upper frame in each figure depicts the characteristic features of the trajectory, the middle one presents the dynamics of a particle passage, and the bottom one corresponds with the particle's probability density at the time point where 50% of the particle escaped from the channel.

Fig. 1 represents the propagation in the simplest system: a perfectly flat trajectory, 40 Å long, under zero external potential and invariable entropic terms along the whole trajectory. In such a system (*left panels* in Fig. 1), a single particle executes a random, unbiased motion, but as the exit port is on the other side of the channel, a gradient of probability density is formed. The highest probability density is at the port of entry, while at the exit port; the probability density is diminishingly small. This gradient is sufficient to drive a particle flux and after $N_{1/2} \sim 700$ random steps, the particle's probability had diminished to 50%. At that time point, the probability density map revealed that the highest value is still at the point of origin. Running the same scenario under an external electrostatic field (*right panels* of Fig. 1) accelerates the eviction of the particle from the channel, and shifts the point of maximal probability density (at $N_{1/2}$) toward the exit port.

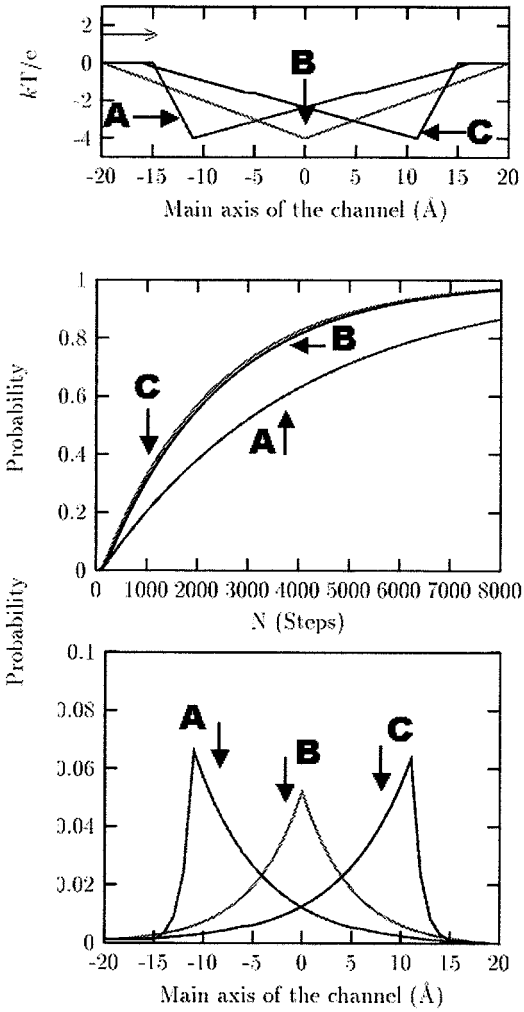

FIGURE 2 Propagation of a particle along a schematic trajectory having an internal electrostatic gradient in the absence of external electric field. Three systems are under investigation, all having a single potential minimum of 4 k_BT, but the location varies in place, as indicated by the letters *A–C*. The middle panel depicts the eviction dynamics; the accumulation of the particle's probability density past the exit port is presented as a function of the number of random steps taken by the system. Please note that the curves calculated for systems *B* and *C* are practically identical, and significantly faster than the dynamics of system *A*. The bottom panel presents the probability density along the channel after $N_{1/2}$ random steps.

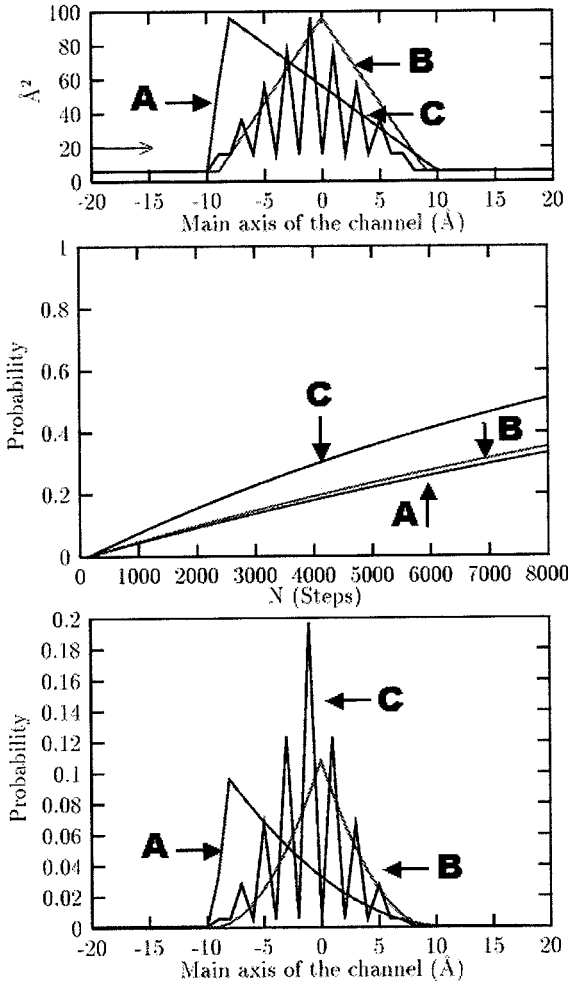

FIGURE 3 Propagation of a particle along a schematic trajectory having an uneven entropy term in the absence of an external electric field. Three systems are under investigation and differ in the distribution of the entropy term (S_i value) along the trajectory. The shape of the S_i function along the trajectory is presented in the top panel, the eviction dynamics in the middle panel, and the probability density profile for the three systems after $N_{1/2}$ random steps is given in the bottom panel.

A more complex system is exemplified in Fig. 2, where the internal electrostatic potential profile is not flat. Three electrostatic profiles are presented in the figure, all having a single minimum of equal depth, but the location varies in the three scenarios. In one case the minimum is close to the origin, while in the other two it gradually shifted toward the exit (*top panel*). Thus, in the first case, the particle will first propagate down a short steep gradient followed by a long, yet mild up-gradient. In the second case, both down- and up-gradients are of equal steepness, while in the third scenario the final phase of the passage will be against a steep but short gradient. The eviction dynamics of the three cases (Fig. 2, *middle panel*) indicate that, contrary to the intuitive guess, the fastest dynamics were noticed when the maxima of the probability density are close to the exit port (*bottom panel*). The dynamics for cases 2 and 3 are almost identical, demonstrating the synergy between the transition probability (which decreases with the steepness of the gradient) and the proximity of the site of maximal probability density to the exit port.

Fig. 3 depicts the dynamics of three trajectories that are flat with respect to the electrostatic potential, but have variable entropy along their length. Of the three calculated dynamics, the one where the trajectory is enriched by clusters of sites having high probability density is significantly faster than the other two.

These computations emphasize the main feature of the propagation system: the local flux between two adjacent sites along the trajectory is the product of the transition probability multiplied by the probability density. Thus, enrichment of the probability density at a site will increase the flux in its vicinity. In the remainder of this study we shall apply the same procedure for propagation of positive or negative charges along the trajectories calculated for five large-pore channels.

The electrostatic potential of the PhoE channel

The electrostatic potential inside the PhoE channel was calculated as described in the accompanying article using the structure of the protein as the sole input. The dielectric constant of the intra-channel space was taken as $\epsilon_{\text{intra-cavity}} = 50$ and for the bulk water $\epsilon = 80$. In accordance with the electrolyte concentration used in single-channel conductance measurements, the electrostatic potentials were calculated for a solution containing 1 M of 1:1 electrolyte, where the Debye screening length is $\kappa^{-1} = 3$ Å. The intensive ionic screening reduces the potential to values much smaller than those reported in the accompanying article ($I = 10$ μM) and accordingly, the potential gradients are also milder.

Fig. 4 depicts a series of potential maps evenly spaced at 4-Å intervals along the z axis of the PhoE channel. The calculations were made at 0.33 Å resolution, but for the sake of presentation the maps are at 4-Å intervals. The map at $Z = -20$ corresponds with the location where the trimeric structure forms a common vestibule. A narrow, intra-protein channel extends from $Z = -6$ up to $Z = 16$. From there on, the channel flares again to form the periplasmic vestibule. As our interest was focused on the ion passage inside the channel, and not on the bulk-vestibule junction, the electrostatic potential for the sections where the channel merges with the bulk ($Z < -22$ and $Z > 25$) were not calculated, and the propagation was initiated from either $Z = -22$ or $Z = 25$.

The width of the channel at its narrowest section, measured as the distance between the van der Waals boundaries of the protein, is 6 Å (see the red contour in the map at $Z = 0$). However, considering that a 2 Å exclusion radius defined the ion accessible space, the channel appears to be much narrower.

The calculations of the electrostatic potential were carried out for a static protein model, taken from the PBD coordinates, and no structure fluctuations were considered. As will be shown below, the flux calculated for the static model yields rates compatible with the single-channel conductance.

Generation of the ionic trajectories

The ionic trajectories were calculated according to the algorithm that was detailed in the preceding manuscript. In the first phase, the energy profile was checked for the presence of ionic traps, such as the one presented in Fig. 5. The two frames in the figure depict the electrostatic potentials calculated for negative (*top*) and positive (*bottom*) particles. The dotted line in the top frame exhibits a relatively flat potential profile, except for a single steep well, at $Z = 8$, whose potential is $\sim 3\ k_B T$ below the level of its adjacent sites. Any anion propagating along the trajectory could be stuck in the trap, increasing its probability density by ~20-fold with respect to the adjacent sites. The interaction between the propagating particle and the sites on the channel's surface was already reported in the accompanying article, where the single released proton reacted with the numerous carboxylates and was removed from the system for a period longer than the observation time. In contrast to the above system, the single-channel conductance measurements were carried out in 1 M electrolyte solutions, and any site having high affinity for ions was occupied by the appropriate charged particle. For this reason we introduced an explicit Cl^- anion at $Z = -8$ and recalculated the potential maps and trajectories for both negative and positive particles. The continuous line in Fig. 5, *top*, corresponding with the potentials calculated after the insertion of the explicit anion, demonstrates that the insertion of a negative charge had eliminated the trap and replaced it by a small mound ($\sim 1\ k_B T$) that hardly affects the propagation dynamics.

The electrostatic profiles for a positive particle, depicted in Fig. 5, *bottom* either before (*dotted line*) or after (*continuous line*) the insertion of the negative charge, are practically identical. Apparently, the combination of the high charge density inside the channel, together with the intensive ionic screening, damps the local electric field so that the contribution of the explicit anion to the positive particle trajectory is vanishingly small. The search for traps was routinely implemented for all channels reported below, but found only at the PhoE structure.

The trajectories for positive and negative particles for five large-pore channel proteins, PhoE, OmpF, and the WT form of the general diffusion porins of *R. blastica* (1PRN), were calculated by the PTTS algorithm and are presented in Fig. 6. For each channel, two trajectories are depicted: the one in red is for a negative particle and the one in blue for a positive one. The trajectories follow distorted pathways that mostly adhere, at a distance of ion exclusion, to the charges fixed to the channel's surface. In some sites the trajectory expands, reflecting a shallow potential surface with a high entropic term; in other sections the trajectory is narrow, having a cross-section not larger than that of a water molecule (set as a minimum value). The figure also depicts the energy profiles of the channels for positive and negative particles in blue and red, respectively. The potentials presented in the figure are a linear combination of the internal field, determined by the charge distribution along the channel, plus an external driving potential that was used in the

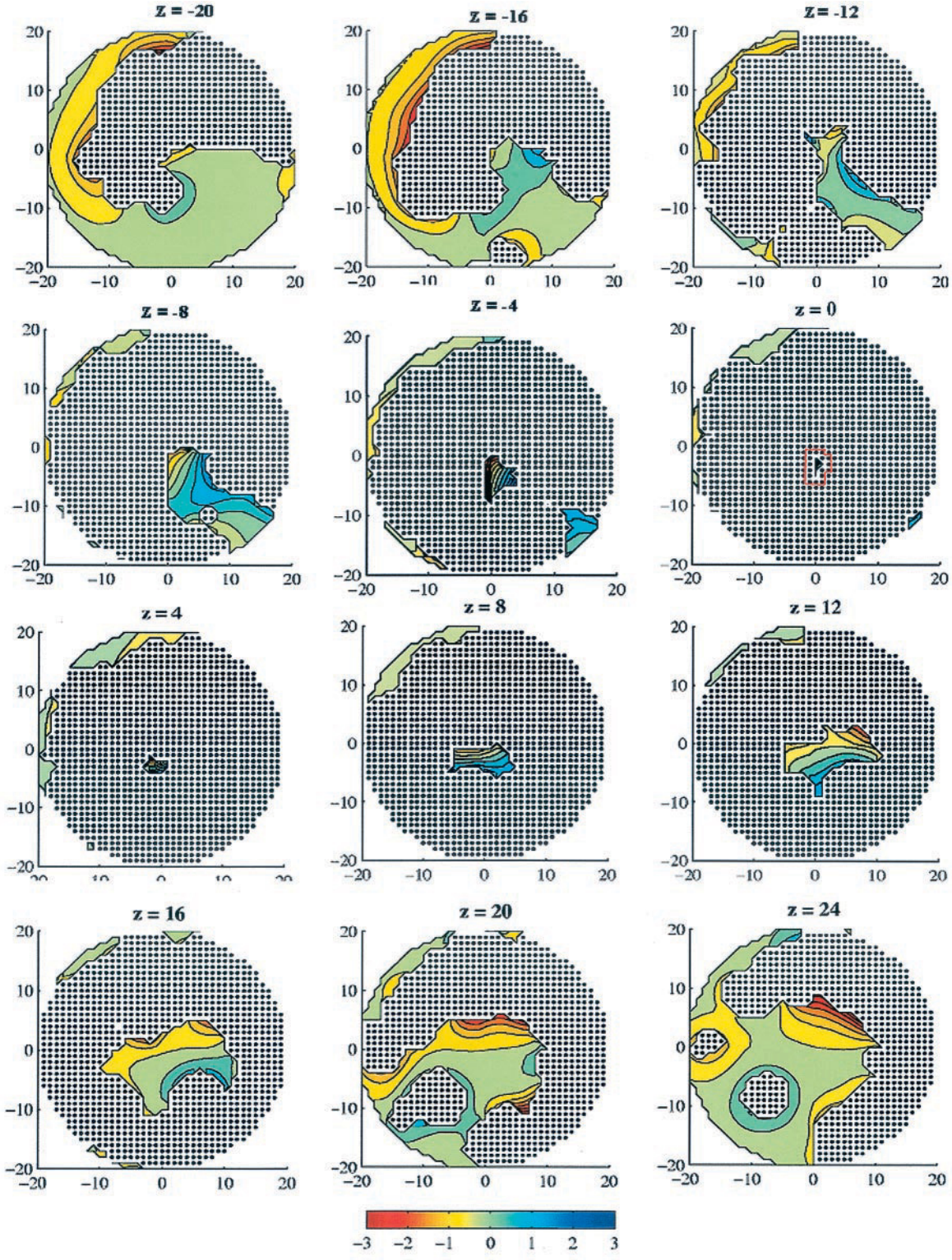

FIGURE 4 The electrostatic potential maps of cross-sections along the PhoE channel. The electrostatic potentials were calculated by the DelPhi program using the detailed structure of the protein and ionic strength of a 1 M solution of 1:1 electrolyte. The maps are presented sequentially, starting from the extracellular side ($Z = -20$) at 4-Å intervals toward the periplasmic side.

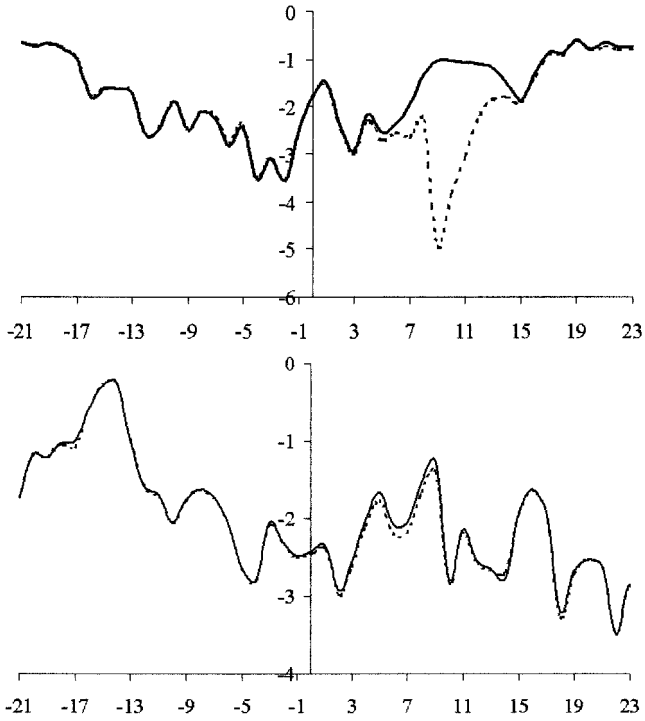

FIGURE 5 The profile of the electrostatic potential along the trajectories calculated for negative (*top frame*) and positive (*bottom frame*) particles along the PhoE channel. The dotted and continuous lines represent, respectively, the potentials as calculated before and after the insertion of an explicit Cl^- anion at the site of $Z = 8$. For details see text.

single-channel conductance measurements (100 mV for PhoE (Vangelder et al., 1997) and OmpF (Bauer et al., 1989) and 20 mV for the 1PRN structure (Schmid et al., 1998)). Thus it is a real presentation of the roughness of the path.

Evaluation of the trajectory profiles reveals that the eyelet region ($-3 \leq Z \leq 3$) does not exhibit distinguished selective features in any of them, the width of the trajectories is constant, and the electrostatic potential does not exhibit any steep gradients that function as rate-limiting steps. Thus, the flux through the channel is a function of the ensemble of transition probabilities, and no specific rate-limiting step can be identified. In the absence of a rate-limiting step, the overall flux can be derived by numeric propagation of a charged particle along the trajectory, as demonstrated above for the test cases (Figs. 1–3).

Propagation of charges along the channel

The propagation dynamics of positive and negative particles in the PhoE channel, as calculated for two possible orientations of the protein in the membrane, are presented in Fig. 7. Four scenarios are presented in this figure, corresponding with the partial fluxes calculated for the two orientations in the membrane and the two ports of entry (extracellular and periplasmic vestibules) In frames *A* and *D* the ions enter the channel space from the extracellular port, while in frames *B* and *C* the entry is from the periplasmic side. The passing ions in frames *B* and *C* are positive, while the propagation dynamics of the negative particles are presented in frames *B* and *D*. The electrostatic profiles are given at the bottom of each frame and are the sum of the internal plus the external fields.

Comparison of the calculated dynamics reveals a great difference between the two scenarios. In the case of a positive particle driven by a net field of 100 mV (Fig. 7 *A*), the intra-channel probability density was reduced to 50% after 950 random steps, while the negative particle (*B*) required $N_{1/2} = 9700$. Inversion of the protein's orientation (*C* and *D*) generated a new pattern of flux; the positive particle still propagated at the same rate, but the rate of the negative particle had increased by the field reversal and its value is $N_{1/2} = 3700$.

The clearance times for the four scenarios are given in Table 1. The wide variation in the values demonstrates that the electrostatic profile and entropy terms provide a fine mechanism that controls the velocity of charged particle propagation through the channels. The conversion of the four individual fluxes into a term that corresponds with the measured current of the unoriented large-pore channel, where both cations and anions enter the pore from both sides, is given in the last three columns of the table. The $N_{1/2}$ represents the clearance rate measured for each frame in Fig. 5. $N^*_{1/2}$ is the summation of the flux calculated for the two ions at each orientation, while the last term, $\underline{N}^*_{1/2}$, corresponds with the average flux, which is equivalent to the average passage time calculated from single channel conductance measurements.

The ionic mobility in the channel

The conversion of the dimensionless parameter $N^*_{1/2}$ into time units was attained by comparison with the measured ionic mobilities in the channel. The single-channel conductance of the PhoE monomer was measured as 0.63 nS (Vangelder et al., 1996). Under a driving potential of $\Delta V =$ 100 mV, this conductance is equivalent to a flux of 3.9×10^8 ions s^{-1} and an average passage time of $\tau = 2.5$ ns. Approximating a channel's length of $L = 45$ Å, the calculated mobility of an average ion in the channel is given by $\mu = (L/\tau)/(\Delta V/L) = 8 \times 10^{-4}$ ($cm^2\ s^{-1}\ V^{-1}$). This value is practically identical with the mobility calculated for a 1 M solution of NaCl (8.7×10^{-4} $cm^2\ s^{-1}\ V^{-1}$ (Robinson and Stokes, 1959). The standard mobility of ions in the PhoE channel implies that the diffusion coefficients of the ions in the channel are comparable with their diffusion coefficient as measured in water ($D = 1.48$ and 1.89×10^5 $cm^2\ s^{-1}$ in 1 M solution of NaCl and KCl, respectively Robinson and

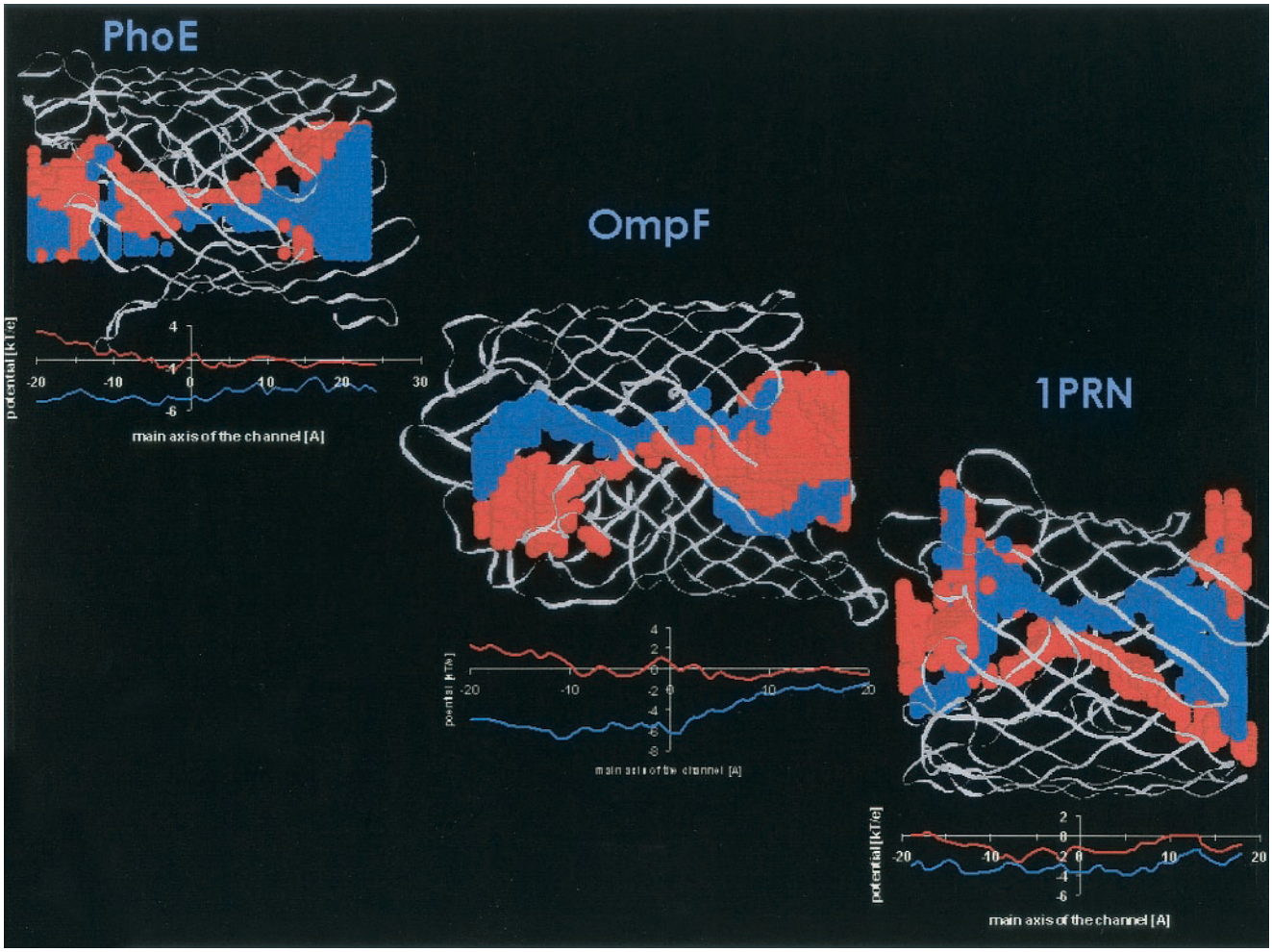

FIGURE 6 The most probable trajectories for ion passage through the PhoE, OmpF, and the WT form of the *R. blastica* general purpose porin (1PRN). The trajectories are presented as spheres ($R = 1$ Å) colored in red for negative particles and blue for positive ones. Below each image is the electrostatic potential profile calculated for a 1 M solution of 1:1 electrolyte and an external field of −100 mV (PhoE and OmpF) or −20 mV (1PRN). The potential of the periplasmic side is set at 0.

Stokes, 1959, no. 1762, Appendix 11.2). On the basis of the diffusion coefficient, the time frame of a single random step was determined to be $\Delta t = \Delta r^2/2D \sim 4$ ps ($\Delta r = 1$ Å). This conversion factor will be used below to calculate the passage time through the channel.

It is of interest to point out that the Ohmic calculation of the channel's conductance as the product of the pore's volume (Smart et al., 1997) and the conductance of the salt solution had led in the past to the conclusion that the diffusion coefficient inside the intra-cavity space is only ~30% of the bulk value (Benz and Buer, 1988). Most likely, this discrepancy is a consequence of the assumption that the total volume of the channel's aqueous space is fully conductive. The adoption of the trajectory concept, which reduces the conductive pathway to a small fraction of the total intra-cavity space, eliminates the discrepancy between the bulk and channel diffusion coefficient.

The average passage time in the large-pore channel

The intra-channel trajectories were calculated for the OmfP, the WT protein of the *R. blastica* general diffusion porin (corresponding with the 1PRN entry of the protein data bank), and two mutants of the same protein, E99W/A116W (2PRN) and K50A/R52A (6PRN). The propagation of the charged particle through the channels was carried out as described for the PhoE and the $\underline{N}^*_{1/2}$ values summed up in Table 2, using a time frame of 4 ps/step.

The first three columns in the table denote the measured single-channel conductance of the protein, the voltage applied in the experiment, and the average passage time. The next two columns refer to the calculated values: the $\underline{N}^*_{1/2}$ value, as calculated in Table 1, and the first passage time, based on the approximation of 4 ps per step. The last

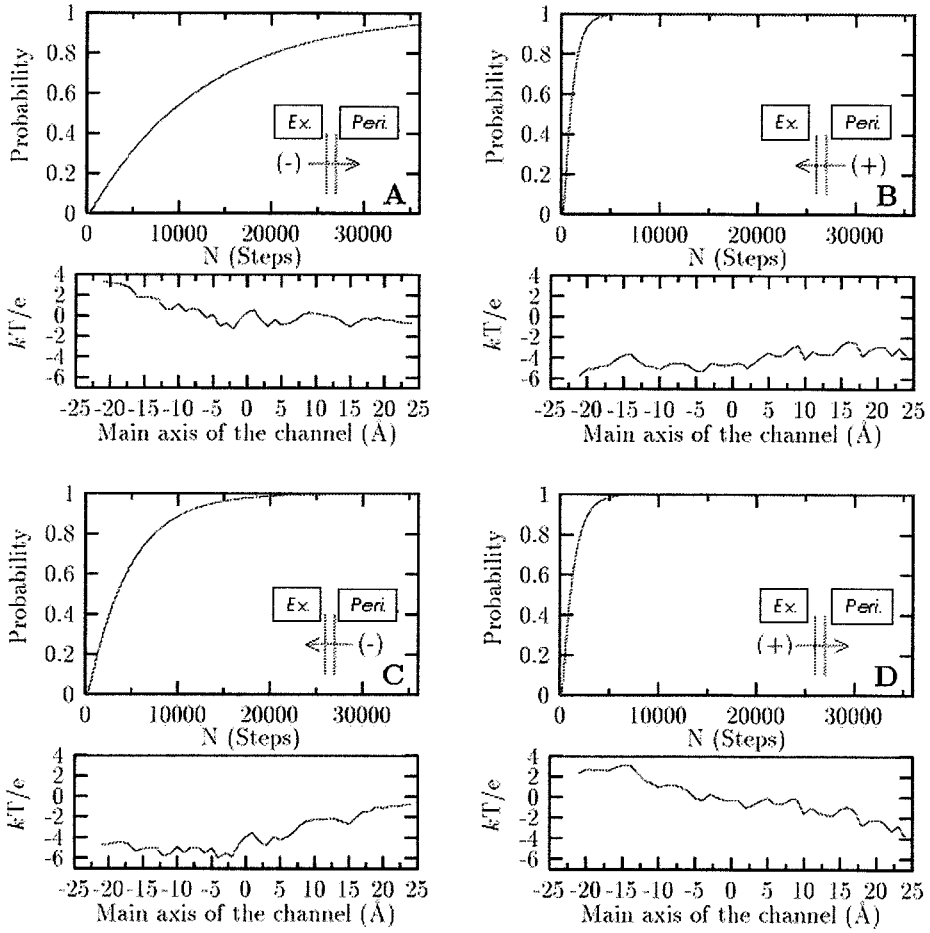

FIGURE 7 Propagation dynamics of positive and negative particles through the PhoE channel under a 100 mV driving potential. The scenario is divided into four cases. Panels *A* and *B* depict the eviction dynamics of negative and positive particles moving through the channel protein in one orientation of the protein across the membrane, while frames *C* and *D* are the fluxes for the reverse orientation of the protein. Frames *A* and *C* depict the dynamics calculated for a negative particle. Frames *B* and *D* are for a positive particle. The ordinates denote the accumulation of the probability density past the exit ports and the abscissa is the number of random steps. Under each of the frames depicting the dynamics is the profile (in *kT* units) of the electrostatic potential along the trajectory.

column is the ratio between the calculated and the experimental values. Of the five systems we note a close correlation between the measured and calculated passage times. In the only case where the ratio between the measured and calculated time constants is large (185%), the mutation consists of inserting two protruding tryptophan residues into the channel's lumen, reducing the passage to <5 Å. The passage of ions through such a narrow gate is already sensitive to the protein's dynamics. It is plausible that, during the structural fluctuations of the protein, the pore may have a larger diameter than that determined for the crystalline porin. The ion flux through the other mutant K50A/R52A, which is a substitution that alters the electrostatic potential in the channel, was accurately predicted by our calculations. Thus, the model we use is valid as long as the protein dynamics are not crucial for the ion passage.

TABLE 1 The passage parameters of charged particles through the PhoE channel

Scenario	Charge	k_{res}	$N_{1/2}$	$N^*_{1/2}$	$\underline{N}^*_{1/2}$
A	−	2.8×10^{11}	9712		
B	+	2.3×10^{8}	950	865	
C	−	4.9×10^{9}	3700		850
D	+	9.7×10^{10}	1110	835	

The calculations were made for a single charged particle along the trajectory corresponding with its charge under a driving potential of either +100 or −100 mV. The scenarios pertinent for the calculations are presented in Fig. 6.

Prediction of the ionic selectivity of the large-pore channel

The selectivity of ion channels is a product of the interaction between the structural elements and the local electrostatic fields with the charge and hydration layer of the permeating ion. For these reasons, ions that differ in their ionic radius or solvation energy (such as Na^+, K^+, and Li^+ or Cl^- vs. acetate) are discriminated by the channel (Struyve et al., 1993). Our intention was to find out whether the propagating program, when operating under conditions analogous to those used for measuring the ionic selectivity, also reveals the uneven rate of passage of anions versus cations.

The ionic selectivity of a large-pore channel is calculated from the zero-current potential that is built up under an electrolyte concentration gradient (100 mM vs. 10 mM) maintained across the membrane (Benz and Buer, 1988).

TABLE 2 Comparison between the measured and predicted passage time of ions in large-pore channels

Channel	Conductance (nS)	ΔV (mV)	τ^* (ns)	$N^*_{1/2}$	$\tau^\dagger$ (ns)	$\tau^\dagger/\tau^*$
PhoE	0.63‡	100	2.5	850	3.4	136%
OmfP	0.84§	100	1.8	550	2.0	110%
R. blastica porin WT	1.3¶	20	6.0	1047	4.2	70%
R. blastica porin E99W/A116W	0.7¶	20	11.3	5288	21	185%
R. blastica porin K50A/R52A	1.4¶	20	5.6	1574	6.3	112%

*Passage time determined experimentally.
†Passage time calculated from the propagation dynamics.
‡Vangelder et al., 1997.
§Bauer et al., 1989.
¶Schmidt et al., 1998.

Precise reconstruction of the zero current potential by the propagation method is too complex, and an alternative mechanism to simulate the selectivity was searched for. The selected method was to drive the charged particles by a concentration gradient and to quantitate the selectivity by the ratio of the calculated passage times predicted for negative versus positive particles. The calculation of the intracavity electrostatic potential was carried out at an ionic strength of 100 mM, and the low salt concentration (10 mM) on the periplasmic side of the channel was substituted by a scenario assuming that 10% of the particles that reached the exit port would be reflected back into the channel's lumen. This scenario is a fair approximation for the initial flux before the back potential is established. The calculations were carried out for PhoE, OmpF, and the WT general diffusion porin channels. The ratio of the passage times for positive and negative particles, as calculated for PhoE, OmpF, and the WT general diffusion porin, were 2.4, 4.7, and 4.8, while the measured charge preferences were 0.3 (Bauer et al., 1989), 4.0 (Delcour, 1997), and 13 (Schmid et al., 1998), respectively. The fact that the calculations with the potential profile of the trajectory yielded selectivities that differ from the measured ones emphasizes the crucial role of the screening at the vestibule (Chung et al., 1998; Hoyles et al., 1996; Jordan, 1984; Kuyucak et al., 1998). The PSST program had been deliberately made to ignore the vestibular screening and is controlled only by the forces operating inside the channel. Indeed, the Brownian motion simulations of Phale (Phale et al., 2001) and Schirmer (Schirmer and Phale, 1999), where the screening at the entrance was a major factor controlling the probability of ions to transverse the width of the membrane, accurately predicted the selectivity of the channel, yet it must be recalled that the Brownian motion simulations are inadequate for reconstructing the dynamics of ion passage. Thus, the procedure presented here, together with the Brownian motion calculation, is complementary in nature; each mode of calculation emphasizes one aspect of the complex phenomenon of ion permeation through large-pore channels.

CONCLUSIONS

In the present study we used the PSST algorithm, developed for the reconstruction of a single proton diffusion in the PhoE channel, to simulate ion flux in large-pore channels. The calculation disregarded many features of the protein and the solvent: 1) the protein dynamics were ignored, assuming the structure was fixed in time; 2) the solvent was replaced by a continuum model whose dielectric constant was set equal to that obtained upon the refinement of the proton-PhoE system (see accompanying article); 3) of the many ions present in the channel space, all but one are represented through the attenuation of the electrostatic potentials by the ionic strength term; and 4) the calculation were also carried out as if the charge of the propagating particle does not affect the electrostatic potential, nor does it interact with the counterion in the channel, although the probability of cation anion interactions are not negligible within the constriction zone.

Despite all of the negligence, the calculations were able to reproduce many features of large-pore channels; the passage times were consistent with the single-channel conductance values of five proteins and the system exhibited selectivity and even the rectification capacity of the channels, where the currents flowing under reversed polarity are not identical (Vangelder et al., 1997). Finally, the computation time of the propagation is extremely short, taking not more than a few tens of seconds' calculation time on an up-to-date workstation.

The key feature of the PSST algorithm is the reduction of the dimensionality of the diffusion space from three to one. The myriad interactions between all fixed charges with the mobile ions are condensed into potential maps, through which a single trajectory is projected. This operation substitutes the diffusion space for a linear array of sites that are connected by transition probability terms. The combination of the transition probabilities, which are time-invariable parameters, with the probability density at each site, generates the local flux. All local fluxes are inherently linked through the law of conservation of mass, thus the overall

flux is affected by all local ones. For this reason, even though none of the sites along the trajectories can be considered as the rate-limiting step, selective mutations affect the flux through the channel. Most likely, the treatment of the whole channel as a functional ensemble compensated for all the approximations incorporated in the model, producing an efficient model for calculation of ion flux through large-pore channels.

The research in the Laser Laboratory for Fast reactions in Biology was supported by Israeli Science Foundation Research Grant 427/01-1 and German Israeli Foundation for Research and Development Grant I-594-140.09/98).

REFERENCES

Agmon, N. 1988. Geminate recombination in proton-transfer reactions. III. Kinetics and equilibrium inside a finite sphere. *J. Chem. Phys.* 88: 5639–5642.

Agmon, N., E. Pines, and D. Huppert. 1988. Geminate recombination in proton-transfer reactions. II. Comparison of diffusional and kinetic schemes. *J. Chem. Phys.* 88:5631–5638.

Agmon, N., and A. Szabo. 1990. Theory of reversible diffusion-influenced reaction. *J. Chem. Phys.* 92:5270–5284.

Bauer, K., M. Struyve, D. Bosch, R. Benz, and J. Tommassen. 1989. One single lysine residue is responsible for the special interaction between polyphosphate and the outer membrane porin PhoE of *Escherichia coli*. *J. Biol. Chem.* 264:16393–16398.

Benz, R., and K. Buer. 1988. Permeation of hydrophilic molecules through the outer membrane of Gram-negative bacteria. *Eur. J. Biochem.* 176: 19–21.

Benz, R., A. Schmid, and R. E. Hancock. 1985. Ion selectivity of Gram-negative bacterial porins. *J. Bacteriol.* 162:722–727.

Benz, R., A. Schmid, P. Van der Ley, and J. Tommassen. 1989. Molecular basis of porin selectivity: membrane experiments with OmpC- PhoE and OmpF-PhoE hybrid proteins of *Escherichia coli* K-12. *Biochim. Biophys. Acta.* 981:8–14.

Breed, J. S., R. I. D. Kerr, and M. S. P. Sansim. 1996. Molecular dynamics simulations of water within models of ion channels. *Biophys. J.* 70: 1643–1661.

Chung, S. H., M. Hoyles, T. Allen, and S. Kuyucak. 1998. Study of ionic currents across a model membrane channel using Brownian dynamics. *Biophys. J.* 75:793–809.

Delcour, A. H. 1997. Function and modulation of bacterial porins: insights from electrophysiology. *FEMS Microbiol Lett.* 151:115–123.

Eppens, E. F., N. Saint, P. Vangelder, R. Vanboxtel, and J. Tommassen. 1997. Role of the constriction loop in the gating of outer-membrane porin PhoE of *Escherichia coli*. *FEBS Lett.* 415:317–320.

Hoyles, M., S. Kuyucak, and S. H. Chung. 1996. Energy barrier presented to ions by the vestibule of the biological membrane channel. *Biophys. J.* 70:1628–1642.

Jakobsson, E. 1998. Using theory and simulation to understand permeation and selectivity in ion channels. *Methods.* 14:342–351.

Jordan, C. P. 1984. Effect of pore structure on energy barriers and applied voltage profile. *Biophys. J.* 45:1091–1100.

Kurnikova, M. G., R. D. Coalson, P. Graf, and A. Nitzan. 1999. A lattice relaxation algorithm for three-dimensional Poisson-Nernst-Planck theory with application to ion transport through the gramicidin A channel. *Biophys. J.* 76:642–656.

Kuyucak, S., M. Hoyles, and S. H. Chung. 1998. Analytical solutions of Poisson's equation for realistic geometrical shapes of membrane ion channels. *Biophys. J.* 74:22–36.

Menzl, K., E. Maier, T. Chakraborty, and R. Benz. 1996. HlyA hemolysin of *Vibrio cholerae* O1 biotype E1 Tor. Identification of the hemolytic complex and evidence for the formation of anion-selective ion-permeable channels. *Eur. J. Biochem.* 240:646–654.

Partenski, M. B., and C. P. Jordan. 1992. Theoretical perspectives on ion channel electrostatics: continuum and microscopic approaches. *Q. Rev. Biophys.* 25:477–510.

Phale, P. S., A. Philippsen, C. Widmer, V. P. Phale, J. P. Rosenbusch, and T. Schirmer. 2001. Role of charged residues at the Ompf porin channel constriction probed by mutagenesis and simulation. *Biochemistry.* 40: 6319–6325.

Pomes, R., and B. Roux. 1996. Structure and dynamics of a proton wire: a theoretical study of H^+ translocation along the single-file water chain in the gramicidin A channel. *Biophys. J.* 71:19–39.

Robinson, R. A., and R. H. Stokes. 1959. Electrolyte Solutions. 2nd edition. Butterworths Publications Ltd., London.

Schirmer, T., and P. S. Phale. 1999. Brownian dynamics simulation of ion flow through porin channels. *J. Mol. Biol.* 294:1159–1167.

Schmid, B., L. Maveyraud, M. Kromer, and G. E. Schulz. 1998. Porin mutants with new channel properties. *Protein Sci.* 7:1603–1611.

Smart, O. S., J. Breed, G. R. Smith, and M. S. Sansom. 1997. A novel method for structure-based prediction of ion channel. *Biophys. J.* 72: 1109–1126.

Struyve, M., J. Visser, H. Adriaanse, R. Benz, and J. Tommassen. 1993. Topology of PhoE porin: the "eyelet" region. *Mol. Microbiol.* 7:131–140.

Vangelder, P., N. Saint, R. Vanboxtel, J. P. Rosenbusch, and J. Tommassen. 1997. Pore functioning of outer-membrane protein PhoE of *Escherichia coli*: mutagenesis of the constriction loop L3. *Protein Eng.* 10:699–706.

Vangelder, P., M. Steiert, M. Elkhattabi, J. P. Rosenbusch, and J. Tommassen. 1996. Structural and functional characterization of a His-tagged PhoE pore protein of *Escherichia coli. Biochem. Biophys. Res. Commun.* 229:869–875.